Synthesis and Rheological Properties of Nickel-Zinc Ferrite Polymer Nanocomposites

S. Jebelli Moeen,[1,2] M. R. Vaezi,[1] A. A. Yousefi,[3] E. Ghasemi[2]

[1]*Division of Advanced Materials, Material and Energy Research Center (MERC), Karaj, Iran*
[2]*Department of Inorganic Pigment and Glazes, Institute for Color Science and Technology (ICST), Tehran 1668814811, Iran*
[3]*Department of Plastics Engineering, Iran Polymer and Petrochemical Institute (IPPI), Tehran 14965-115, Iran*

Received 24 August 2010; accepted 11 March 2011
DOI 10.1002/app.34492
Published online 30 August 2011 in Wiley Online Library (wileyonlinelibrary.com).

ABSTRACT: In this work, the ferrimagnetic nickel-zinc ferrite nanopowder was synthesized via citrate-ethylene glycol processing, followed by the preparation of the epoxy-based nanocomposite. The materials were characterized using X-ray diffraction (XRD), simultaneous thermal analysis (STA), alternative gradient force magnetometer (AGFM), scanning electron microscopy (SEM) and transmission electron microscopy (TEM). The results showed that the sample calcined at 1000°C for 1 h had the best crystallinity, and the calculated crystallite size of this sample was ~ 105 nm. The rheological properties and the magnetoviscous effect of the nanocomposites were studied by a standard rotating rheometer. The effects of the magnetic fields and shear rate with respect to time were investigated, and the results were discussed in terms of aggregates and magnetic field-induced structures. © 2011 Wiley Periodicals, Inc. J Appl Polym Sci 123: 2534–2539, 2012

Key words: nanocomposite; magnetoviscous; rheology; nickel-zinc ferrite; newtonian fluid

INTRODUCTION

Research on polymeric nanocomposite materials containing inorganic nanoparticles and organic polymers is a relatively new and unique area in materials science. Nanocomposites containing magnetic nanoparticles attract the most attention because of their extensive application in various fields, such as electromagnetic interference shielding (EMI),[1–4] drug delivery, bioprocessing, medical diagnosis, ferrofluids, drug targeting and magnetic resonance imaging (MRI).[5–8] Among the various magnetic materials, nickel-zinc ferrite is a technologically attractive material, and it was first synthesized 50 years ago. Nickel-zinc ferrite is commercially used as high-frequency ferrites for radio frequency coils and transformer cores. This combination of alloy is found to be the most versatile magnetic materials that is particularly suited for high frequency applications due to its high resistivity.[9,10] To prepare these composites that contain inorganic particles dispersed in polymer matrices, the main methods are *in situ* polymerization, sol-gel processing and direct mixing.[8,11] Intimate relationships exist between the rheology of the polymer and the polymer processing steps.[12] Therefore, having a good understanding of the rheological behavior of the initial components of the composite and their fabrication steps plays an important role in the quality of the final polymeric products. In this paper, nickel-zinc ferrite nanopowders were synthesized by citrate-ethylene glycol processing and were loaded into epoxy. The magnetorheological properties of the resulting nanocomposites were then investigated via rheometry.

Correspondence to: M. R. Vaezi (m_r_vaezi@merc.ac.ir).

Journal of Applied Polymer Science, Vol. 123, 2534–2539 (2012)

EXPERIMENTAL

Materials

All materials, including zinc nitrate, $ZnNO_3{\cdot}6H_2O$, nickel nitrate, $NiNO_3{\cdot}6H_2O$, hydrated iron nitrate, $Fe_2(NO_3)_3{\cdot}9H_2O$, citric acid and ethylene glycol, used in this research were analytical grade and produced by the Merck Company.

Nickel-zinc ferrite was synthesized by a method involving citrate-ethylene precursors. A transparent solution of 1*M* citric acid was mixed with ethylene glycol (with the proportion of 60% acid to 40% ethylene glycol) to prepare the initial solution. Another solution was prepared by dissolving stoichiometric amounts of $NiNO_3{\cdot}6H_2O$, $ZnNO_3{\cdot}6H_2O$ and $Fe_2(NO_3)_3{\cdot}9H_2O$ in deionized water. The two solutions were then admixed and heated to 80°C on a hot plate while stirred. After complete dissolution, the temperature was increased to 90–110°C to

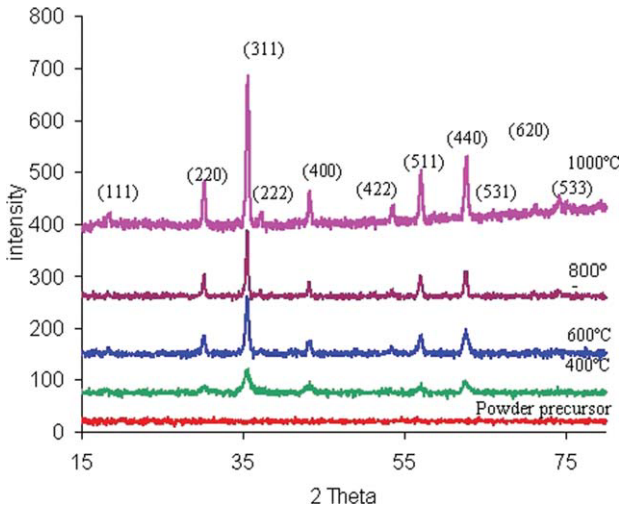

Figure 1 XRD patterns of samples after heat treatment for 1 h at different temperatures. [Color figure can be viewed in the online issue, which is available at wileyonlinelibrary.com.]

promote polyesterification. At the end of the reaction, a brown viscous resin was obtained. Finally, the resin was heated to 300°C and soaked for 1 h. The residual product was divided into four parts and calcined at 400, 600, 800, and 1000°C for 1 h. A homogeneous mixture of nickel-zinc ferrite powders in an epoxy matrix (Epon 828) was prepared with a homogenizer (model UP400S) by mixing for 15 min and was sonicated for 1 h with a sonicator (VIGGEN).

Characterization

Crystallization of the precursor was studied by X-ray diffraction with a Siemens diffractometer (model D-5000) using Cu Kα radiation (λ = 1.5406 Å).

Thermal properties were studied via STA using model PL-1640. The morphology and structure of the nanocomposite were investigated using a Philips scanning electron microscope (model LEO 1455VP) and a Philips transmission electron microscope (model EM208S). Magnetization measurements were carried out with a model 155 alternative gradient force magnetometer at room temperature. The rheological properties of the nanocomposite were measured with a Physica MCR300 rheometer from Anton Paar GmbH. A plate-plate spindle (model PP25-MRD) with a 1.95 cm diameter was employed for all the measurements.

In all rheological tests, the samples were sheared at a shear rate of 1000 s^{-1} for 30 s before measurement. The sample was then allowed to relax for 30 s to achieve steady state. During the rheological measurements, a magnetic field was applied vertically to the sample, and the temperature was adjusted to 25 ± 0.01°C.

RESULTS AND DISCUSSION

Crystalline structure refinement

The XRD patterns of $Zn_{1-x}Ni_xFe_2O_4$ ($x = 0.5$) showed the characteristic reflections of the Fd^3m cubic spinel group as the major phase (Fig. 1). It is obvious that the citrate-ethylene glycol procedure led to the formation of the ferrite spinel at relatively low temperatures. Conventional methods require relatively high temperatures and long heating time to produce the desired material.[13,14] However, the ferrite phase was obtained in a shorter time and at temperatures as low as 400°C using this method. The relatively broad peaks were attributed to the small crystallites.

The mean crystallite size was calculated from (311) peak using Scherrer's formula[15]:

$$D = 0.9\lambda/\beta\cos\theta \quad (1)$$

where D is the average crystallite size in nm, λ is the X-ray wavelength in nm, β is the angular line width at half-maximum intensity and θ is Bragg's angle in degrees.

The calculated crystallite sizes of 30 and 105 nm at 400°C and 1000°C, respectively, could be the result of grain growth.

The TEM and selected area electron diffraction (SAED) patterns of the magnetic particles calcined at 400°C and 1000°C are shown in Figure 2. It is clear that the particle size increased with increasing calcination temperatures. As shown in Figure 2(a), the particle size of the sample synthesized at 400°C was about 50 nm, whereas the sample calcined at 1000°C had larger particle sizes ranging between 100 nm and 200 nm. The difference between the SAED pattern of Figure 2(a,b) was due to the nanocrystalline nature of the spinel structure in the sample calcined at a lower temperature. The seven rings illustrated in both figures were in good agreement with the main peaks of the spinel structure shown in the XRD pattern.

Thermal analysis

Figure 3 shows the results of DTA and TG analysis for the nickel-zinc ferrite precursor. The thermogravimetric curve showed three stages of weight loss. The total weight loss was ~ 90% up to 400°C, which is typical in synthesis processes using polymeric precursors.[16] The first stage of weight loss was related to the elimination of water and adsorbed gases. The second and third weight loss stages were due to the decomposition of organic compounds.[17] The DTA curve revealed a large exothermic peak between 360°C and 400°C.[18] After 400°C, no further weight loss was observed. However, a broad exothermic peak observed between 450°C and 900° indicated the crystallization of the nickel-zinc ferrite phase that confirmed the XRD results of 3.1.

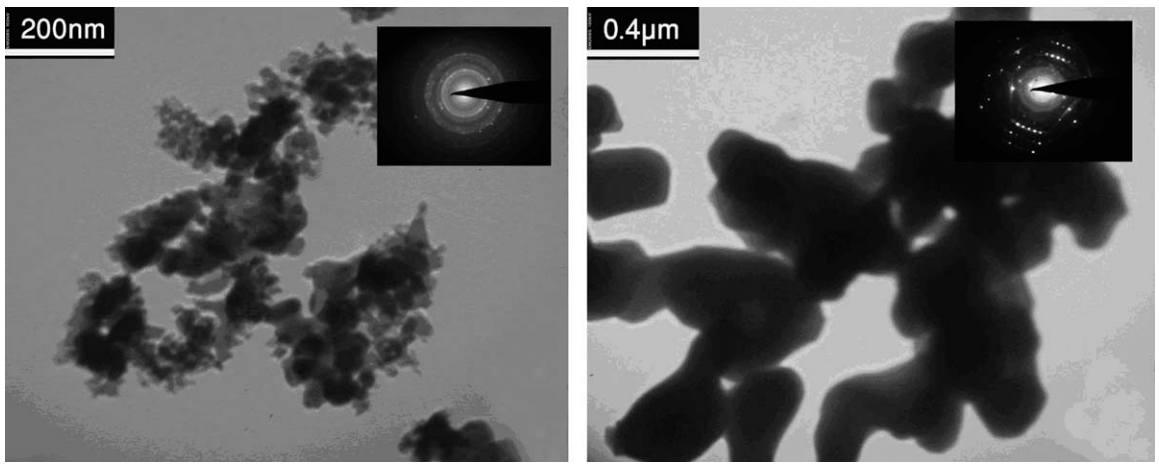

Figure 2 TEM micrographs of the synthesized magnetic particles calcined at (a) 400°C and (b) 1000°C.

Magnetic properties

The magnetization curve at room temperature for the sample treated at 1000°C is shown in Figure 4. This figure indicates the ferrimagnetic behavior of the nickel-zinc ferrite. The values of saturation magnetization (M_s), remnant magnetization (M_r) and coercivity (H_c) were 92.8 emu/g, 10.64 emu/g, and 20 Oe, respectively. The coercivity was noticeably low, and the hysteresis was negligible. The inset shows the fracture of the curve at low applied fields (−100 to +100 Oe), indicating remnant and coercivity of nickel-zinc ferrite.

Rheological properties

The rheological measurements were carried out on a noncrosslinked system to investigate both the effect of powder on the properties of the composite and to highlight the rheomagnetic behavior of the powder. Figure 5 reveals that the behavior of the nanocomposite conforms well to the Bingham model.[19,20] The shear stress of the model is typically represented by $\tau = \tau_0 + \eta_0\dot{\gamma}$, where τ denotes the shear stress, τ_0 is the yield stress, η_0 is the viscosity at zero field and $\dot{\gamma}$ is the shear rate.[21] The conformity to the Bingham model is better at shear rates higher than 10 s^{-1}. The variation of viscosity versus shear rate for epoxy and the nanocomposite is shown in Figure 6. In this figure, the effect of magnetic field on the viscosity can be distinguished more clearly. It can be seen that the base polymer had Newtonian behavior over the experimental shear rate range (0.1 to 1000 s^{-1}), while the composite exhibited shear-thinning behavior in the rate range from 0.1 to 20 s^{-1} and Newtonian behavior at higher shear rates. Generally, the solid particle-particle interactions are the determining factors in the rheological behavior of magnetic fluids.[22] The attractions between the particles lead to the formation of aggregates. Shear stresses can destroy such aggregated structures via increasing shear rate, known as the shear-thinning behavior.[23] On the basis of the results, it can be concluded that the interactions were too weak between the particles to cause aggregation at shear rates higher than

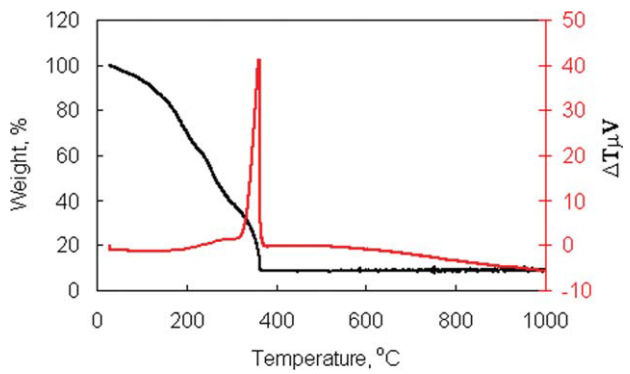

Figure 3 TG and DTA curves for the gel precursor up to 1000°C at a heating rate of 5°C/min. [Color figure can be viewed in the online issue, which is available at wileyonlinelibrary.com.]

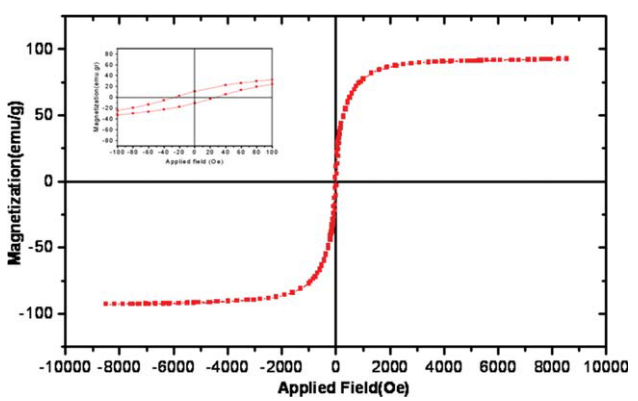

Figure 4 Hysteresis loops of the nickel-zinc ferrite. [Color figure can be viewed in the online issue, which is available at wileyonlinelibrary.com.]

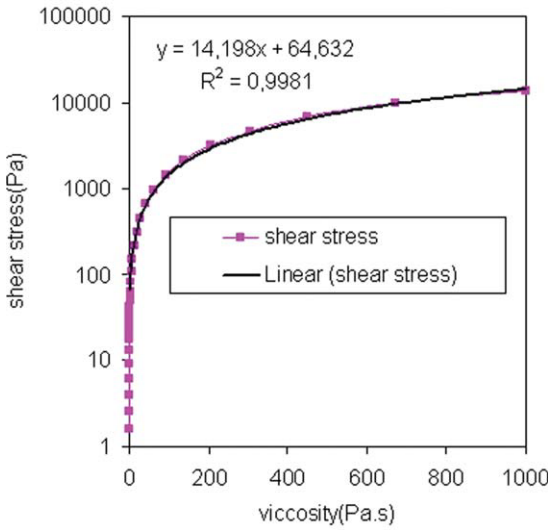

Figure 5 Variation of shear stress with respect to viscosity. [Color figure can be viewed in the online issue, which is available at wileyonlinelibrary.com.]

20 s^{-1}. Therefore, the rheological behavior of the composite transformed from the shear-thinning type to the Newtonian type at higher shear rates.

The initial viscosity increased when the composite was subjected to the magnetic field. This increase was due to the magnetic interactions between the particles and the formation of chain-like structures upon entering the magnetic field. This effect is known as the magnetoviscous effect.[23] The relative viscosity, $\frac{\Delta\eta}{\eta_o} = \frac{\eta-\eta_o}{\eta_o}$, is considered as the main criterion for this effect. In the above equation, η_0 and η represent the viscosity of the ferrofluid before and after application of the magnetic field, respectively. It is worth noting that at low magnetic fields, such as 18 kA/m fields, the Newtonian behavior was observed in the composite as shear rate increased.

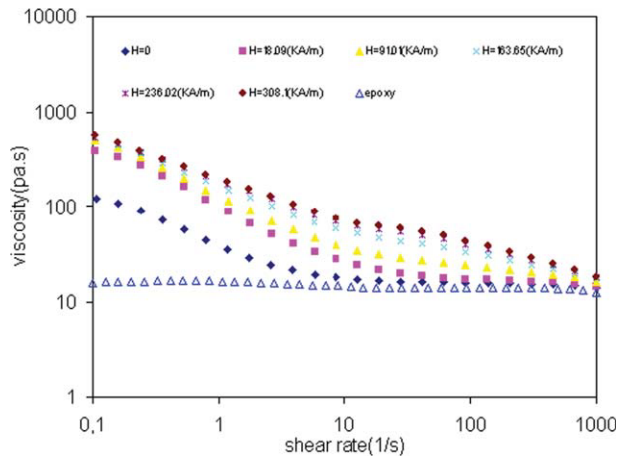

Figure 6 Variation of viscosity with respect to shear rate at different magnetic fields. [Color figure can be viewed in the online issue, which is available at wileyonlinelibrary.com.]

TABLE I
Power-Law Parameters (*k*, *n*) and the Line Regression (R^2) for Composite Calculated from the Shear-Thinning Regions of the Curves

R^2	*n*	*K*	H(KA/m)
0	43.852	0.3001	0.9596
18.09	104.68	0.3909	0.9903
91.01	137.19	0.4303	0.9916
163.65	172.28	0.5095	0.9937
236.02	192.32	0.5467	0.9954
308.1	202.55	0.556	0.9962

However, the composite showed shear-thinning behavior at higher magnetic fields under all shear rates. In these composite systems, different interactions such as magnetic, Van der waals, steric, and depletion forces exist between particles. Among these forces, the magnetic and Van der waals forces are the main contributors to bond formation and particle aggregation.[24]

According to the magnetoviscous theory,[23] the effective number of magnetic particles for chain formation increases with the magnetic field. In other words, the magnetic field enhances the magnetic interactions of the particles. This means that a higher shear stress is required to break up the preformed aggregates. To quantify this effect, the power-law model (Ostwald-de Waele) is ideal for the shear-thinning behavior[25]:

$$\eta = k\dot{\gamma}^{n-1} \tag{2}$$

where η is the apparent viscosity (Pa s), k is the consistency index (Pa s^n), $\dot{\gamma}$ is the shear rate (s^{-1}) and n is the flow behavior index (dimensionless).

The η and k values, seen in Table I, were obtained by fitting the power-law model into the viscosity versus shear rate curves.

As seen in Figure 6, the pure epoxy resin that exhibited Newtonian behavior yielded upon the incorporation of powder in the absence of a magnetic field. This result is a direct indication of structure formation. In the absence of the field, this effect disappeared after 10 s^{-1}. This point indicates the ultimate point of the shear rate where the internal structure of the composite can resist the shear field. Upon applying the magnetic field, the particles that already formed a structure aligned and resisted shear; the structure, in turn, deformed more slowly and sustained for up to 1000 rad/s. It is notable that at low and high magnetic fields, the starting viscosity was almost five to six times greater than that of the composite in the absence of a magnetic field. After applying shear forces, the viscosity decay was slowed down. As seen in Table I, higher magnetic field strengths led to larger shear rate exponents (n).

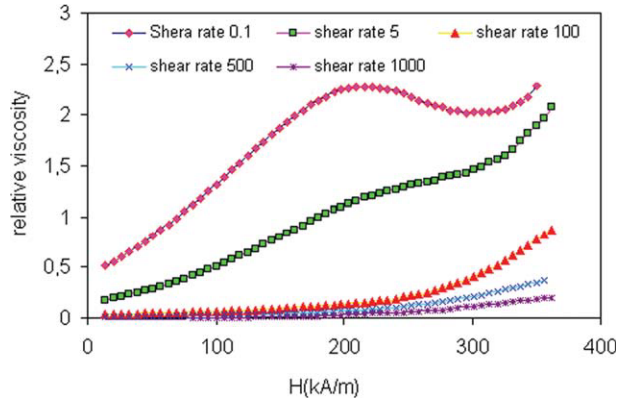

Figure 7 The magnetoviscous effect of the nickel-zinc ferrite composite at various shear rates. [Color figure can be viewed in the online issue, which is available at wileyonlinelibrary.com.]

This trend held true only for range of 0.1–20 $s^{-1}$of shear rate, and thereafter, the behavior of the composites became very composition-dependent. All of these observations show that the composite formed a structure composed of particles that became stronger in the presence of a magnetic field, and the formed structure remained as the applied field strength increased. This change correlated with the n value of the power-law model that governed the viscosity curves.

Figure 7 shows the magnetoviscous effect of the nanocomposite. It is obvious that at low shear rates, this effect increased appreciably with the magnetic field. As mentioned previously, increasing the magnetic field increased particle aggregation and caused the formation of longer chains or larger clusters. However, maintaining these conditions can cause the magnetic particles to drain out from its base fluid, a phenomenon known as the condensation phase transition.[26] When this phenomenon happens, the viscosity of magnetic fluid will decrease, as shown in Figure 7, in which the shear force is applied at a rate of 0.1 s^{-1}. Higher shear rates can improve the homogeneity of the system and can prevent the phase separation caused by the magnetoviscous effect.

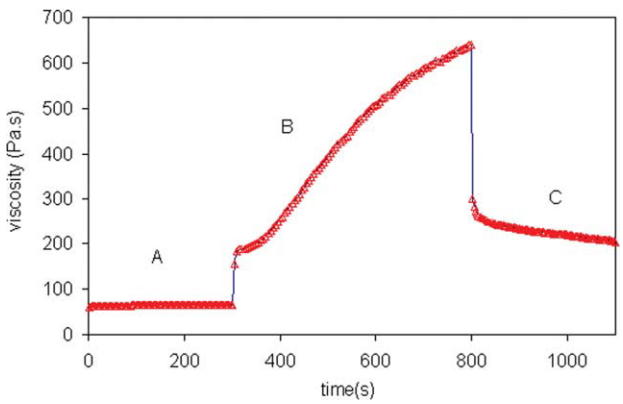

Figure 8 Viscosity of the composite with respect to time. Interval A: H = 0 kA/m; interval B: H = 91 kA/m, interval C: H = 0 kA/m. [Color figure can be viewed in the online issue, which is available at wileyonlinelibrary.com.]

At shear rates higher than 100 s^{-1}, almost no increase in the relative viscosity was observed at magnetic fields lower than 200 kA/m. Thus, the magnetic field-induced structures were not strong enough to resist the applied shear rates. However, the relative viscosity increased at magnetic fields higher than 200 kA/m.

As shown in Figure 8, the time dependency of viscosity at low shear rates was investigated. In this figure, three intervals were observed. In time Zone A, the magnetic field was not applied, and the viscosity of the composite was constant. As the magnetic field was applied, the viscosity increased, as seen in time Zone B, namely, magnetic field-induced structure formed gradually. A sudden increase in the viscosity at the boundary of Zones A and B suggests a rapid formation of a magnetic structure. This formation can be related to the presence of larger particles.[27,28] With the rearrangement of particles and initiation of agglomerates, the interaction between the particles increased gradually. Subsequently, the network of clusters became more extended and the viscosity increased.

When the magnetic field was turned off, the viscosity decreased rapidly. This decrease was related to the distortion of the magnetic field-induced structure. It is notable that in the absence of the magnetic field, the viscosity was higher than the initial viscosity of Zone A. This difference means that some part of the structures formed initially have not yet been destroyed. As the viscosity decreased with time, the remaining agglomerated structures became somewhat unstable and behaved like the iron oxide ferrofluid discussed by Ghasemi et al.[29] Despite the differences between the magnetic fluid systems, mechanisms of aggregate formation and distortion are likely similar.

CONCLUSIONS

Nickel-zinc ferrite nanopowders were synthesized by citrate-ethylene glycol processing, and an epoxy-based nanocomposite was prepared in this work. According to XRD patterns, the crystallization of nickel-zinc ferrite began at 400°C and was completed at 1000°C as crystal growth occurred. It was shown that particle interaction changed the rheological properties of the nanocomposite, which was in good conformity to the Bingham model. At low shear rates without a magnetic field, the nanocomposite exhibited shear-thinning behavior that converted to Newtonian behavior at shear rates higher than

10 s^{-1}. Additionally, the magnetic field enhanced the magnetic interactions between the nanoparticles and caused a six-fold increase in viscosity via the magnetoviscous effect. On the other hand, shear stress reduced the magnetoviscous effect. The extent of changes in the strength of the internal structure in the presence of a magnetic field was quantified by the slope of the power-law region and the corresponding n values. It was shown that the phase separation of the nanocomposite occurred at magnetic fields higher than 200 kA/m. Moreover, the formation and distortion of magnetic field-induced structure was correlated with time.

References

1. Liu, C.; Rondinone, A. J.; Zhang, Z. J Pure Appl Chem 2000, 72, 37.
2. Matsumoto, M.; Miyata, Y. J Appl Phys 2002, 91, 9635.
3. Slama, J.; Gruskova, A.; Vicen, R.; Vicenova, S.; Dosoudil, R.; Franek, J. J Magn Magn Mater 2003, 254, 642.
4. Azhdar, B.; Stenberg, B.; Kari, L. Polym Composites 2008, 29, 252.
5. Pant, P.; Rashmi, R.; Krishna, M.; Negi, P. S.; Ravat, K.; Dhwan, U.; Gupta, S. K.; Suri, D. K. J Magn Magn Mater 1995, 149, 10.
6. Gomez Lopera, S. A.; Plaza, R. C.; Delgado, A. V. Colloid Interface Sci 2001, 240, 40.
7. Arshady, R. Biomaterials 1993, 14, 1.
8. Chae, D. W.; Lee, K. H.; Kim, Y. C. J Polym Sci: Part B: Polym Phys 2006, 44, 371.
9. Wiltshires Pendry, M. C. K.; Young, J. B.; Larkman, I. R.; Gilderdale, D. J.; Hajnal, J. V. Science 2001, 291, 849.
10. Cinibulk, M. K. J Am Ceram Soc 2000, 83, 1276.
11. Chae, D. W.; Kim, B. C. H. Compos Sci Technol 2007, 67, 1348.
12. Han, C. D. Rheology and Processing of Polymeric Materials, Vol 1: Polymer Rheology; Oxford University Press: USA, 2007.
13. Gupta, R. G.; Mendiratta, R. G. J Appl Phys 1977, 48, 845.
14. Gupta, R. G.; Mendiratta, R. G. J Appl Phys 1977, 48, 2998.
15. Cullity, B. D. Elements of X-Ray Diffraction; Addison-Wesley Publishing Company: Reading Massachusetts, 1956; p 259.
16. Gharagozlou, M. J Alloys Compd 2009, 486, 660.
17. Márcia, R.; Silva, S.; Lydianne, C.; Miranda, de., O.; Maria, R. C.-S.; Lima, S. J. G.; Soledade, L. E. B.; Longo, E.; Paskocimas, C. A.; Souza, A. G.; Iêda, M. G. S. J Thermal Anal Calorimetry 2007, 87, 753.
18. Candeia, R. A.; Souza, M. A. F.; Bernardi, M. I. B.; Maestrelli, S. C.; Santos, I. M. G.; Souza, A. G.; Longo, E. J Mater Res Bull 2006, 41, 183.
19. Inoue, H.; Katsumoto, M. J Magn Magn Mater 1993, 125, 377.
20. Bossis, G.; Lacis, S.; Meunier, A.; Volkova, O. J Magn Magn Mater 2002, 252, 224.
21. Mezger, T. G. The Rheology Handbook; Vincent Springer: Hannover, 2002.
22. Thurm, S.; Odenbach, S. Phys Fluids 2003, 15, 1658.
23. Odenbach, S. Magnetoviscous Effects in Ferrofluids; Springer-Verlarg: Berlin Heidelberg, 2002.
24. Birdi, K. C. Handbook of Surface and Colloid Chemistry; 2nd ed. CRC Press: Taylor & Francis Group, 2002.
25. Rauwendaal, C. H. Polymer Extrusion, 3rd ed.; Hanser/Gardner Publications: New York, 1994.
26. Zubarev, A. Y.; Iskakova, L. Y. J Physica A 2005, 349, 1.
27. Odenbach, S. J Phys Condens Matter 2004, 16, 1135.
28. Odenbach, S. J Colloids Surf A Physicochem Eng Aspects 2003, 217, 171.
29. Ghasemi, E.; Mirhabibi, A.; Edrissi, M. J Magn Magn Mater 2008, 320, 2635.